Earth Surf. Dynam. Discuss., 1, 817–853, 2013
www.earth-surf-dynam-discuss.net/1/817/2013/
doi:10.5194/esurfd-1-817-2013

Earth Surface Dynamics Discussions
Open Access

Velocity and concentration profiles of saline and turbidity currents flowing in a straight channel under quasi-uniform conditions

M. Stagnaro and M. Bolla Pittaluga

Department of Civil, Chemical and Environmental Engineering, University of Genova, Genova, Italy

Received: 15 October 2013 – Accepted: 31 October 2013 – Published: 18 November 2013

Correspondence to: M. Stagnaro (mattia.stagnaro@unige.it) and
M. Bolla Pittaluga (michele.bollapittaluga@unige.it)

Published by Copernicus Publications on behalf of the European Geosciences Union.

Abstract

We present a series of detailed experimental observations of saline and turbidity currents flowing in a straight channel. Experiments are performed by continuously feeding the channel with a dense mixture until a quasi-steady configuration is obtained. The flume, 12 m long, is characterized by a concrete fixed bed with a uniform slope of 0.005. Longitudinal velocity profiles are measured in ten cross sections, one meter apart, employing an Ultrasound Doppler Velocimeter Profiler. We also measure the density of the mixture using a rake of siphons sampling at different heights from the bottom in order to obtain the vertical density distributions in a cross sections where the flow already attained a quasi-uniform configuration. We performed 27 experiments changing the flow discharge, the fractional excess density, the character of the current (saline or turbidity) and the roughness of the bed in order to observe the consequences of these variations on the vertical velocity profiles and on the overall characteristics of the flow. Dimensionless velocity profiles under quasi-uniform flow conditions were obtained by scaling longitudinal velocity with its depth averaged value and the vertical coordinate with the flow thickness. They turned out to be influenced by the Reynolds number of the flow, by the relative bed roughness, and by the presence of sediment in suspension. Unexpectedly the densimetric Froude number of the current turned out to have no influence on the dimensionless velocity profiles.

1 Introduction

Turbidity currents flowing in submarine canyons are recognized as preferential conduits for sediment transfer from shallow to deep water. They have a tremendous impact on the deep-sea environment since they affect the ecosystem in various ways, including burial by sediment deposition, exposure by sediment removal, and food supply. Moreover, they are of great engineering relevance due to their ability to reach extremely high velocities that represents a serious geohazard for deep water installations. Addi-

ESURFD
1, 817–853, 2013

tionally, since the majority of sandstones in the geologic record were deposited from rivers or from turbidity currents, they are also extremely significant in the research and exploitation of hydrocarbon reservoirs.

In spite of their relevance, direct observation of the active process has proven extremely difficult since these events are short lived, located at specific sites, unpredictable and, in some circumstances, highly disruptive. A notable exception is the recent field observation performed by Xu et al. (2004), who successfully measured vertical profiles of downstream velocity for four flow events over the space of 1 yr, at three locations down Monterey Canyon, California. Due to these difficulties, the majority of the investigations aimed at understanding the dynamic of turbidity currents has been either through theoretical investigations or through experimental observations.

Altinakar et al. (1996a) performed a large number of experiments on turbidity currents employing either salt or sediments to generate the current. However, they primarily focused their attention on the head rather than on the body of the current. The same authors (Altinakar et al., 1996b) later showed that velocity and concentration distributions could be well represented by similarity profiles independently on the values attained by the main dimensionless parameters (namely densimetric Froude number, Rouse number, relative bed roughness, etc.), once both profiles are scaled with the values attained by the corresponding quantities at the velocity peak. Recently, Sequeiros et al. (2010) somehow contradicted the previous findings showing that the vertical profiles of streamwise flow velocity and fractional excess density, due to salt, salt/suspended sediment or suspended sediment alone, of the flow can be consistently represented depending on the Froude number, the grain size of the bed material and the presence or absence of bed forms. Here we wish to integrate these experimental observations with a new set of observations specifically aimed at make some progress on the dimensionless parameters affecting the shape of velocity and concentration profiles in quasi-uniform turbidity and saline currents. Besides considering the well known influence of the densimetric Froude number and of the relative bed roughness on the vertical profiles, we will also consider the effect of the Rouse and Reynolds number on

ESURFD
1, 817–853, 2013

the vertical structures. This will be done performing a large number of experiments in a straight flume with a fixed sloping bed. The inflow conditions, namely the flow discharge, the fractional density excess, the nature of the current (saline or turbidity), and the bed roughness will be varied over a wide range in order to cover both subcritical and supercritical flows, and both turbulent and nearly laminar flows.

2 Description of the experimental apparatus and procedure

2.1 Experimental apparatus

The experiments are performed in a 30 m long flume, composed by two straight reaches 12 m long joined by a 180° bend with a constant radius of 2.5 m. Inside the plexiglass flume, 0.6 m wide and 0.5 m deep, a constant bottom slope of 0.005 is realized with concrete starting from the inlet cross section of the flume and proceeding 3 m after the bend exit where the bottom keeps horizontal until the end of the flume (Fig. 1). Here we will focus our attention on the first straight reach, only, where the flow is capable to reach a quasi-uniform flow condition.

At the upstream end of the flume a sluice gate is placed to isolate a small portion of the channel where the dense mixture is injected. In this way, the mixture debouching in the inlet chamber is forced to pass through the sluice gate, allowing us to control the upstream flow thickness of the current by changing its height h_0. At the downstream end of the flume a dumping tank with a bottom drain is placed in order to avoid upstream effects induced by the filling of the tank with the dense mixture during the experiment.

The mixture of water and sediment (and/or salt) is created in two mixing tanks, each one approximately equal to 2 m^3 and provided with a mixer which allows the sediment to be taken in suspension and the salt dissolved. The dense fluid is put in the channel using an hydraulic pump through a pipe conduit. The flow rate is measured during the experiment by an orifice flow-meter, and a set of valves in the pipes allow us to set the needed flow discharge before the start of each experiment.

ESURFD
1, 817–853, 2013

A rake of siphons sample the current along the vertical in order to measure the density distribution in cross sections C5 in every run. The siphons are operated manually, and start sampling when the current head reaches the end of the flume and the current reaches quasi-steady conditions. This allows us to obtain the density distribution of the flow body, averaged over the time necessary to get the samples. The siphons are placed at 3, 9, 15, 25, 40, 55, 70, 100, 150, and 200 mm from the bottom, and sample simultaneously. The suction velocity is set such to be similar to the current velocity, in order to obtain realistic samples at the height each siphon is located.

The Ultrasound Doppler Velocity Profiler (UDVP) DOP2000 is employed to measure longitudinal velocity profiles of the flow. We employ 10 probes simultaneously located in different cross sections (from C1 to C10 in Fig. 1) during each experiment. To record the longitudinal profile every probe is placed along the centerline of the flume, partially immersed in the water, pointing upstream and towards the bottom of the flume, with an inclination of 60° with respect to the horizontal (Fig. 2).

2.2 Experiments performed and experimental procedure

In this work we focus our attention on 27 experiments whose main characteristics are summarized in Table 1.

For every experiment the density excess is generated in two different ways depending on the mixture employed. In the case of saline underflows the mixture was obtained by adding salt to clear water, with a small percentage of sediment, added to the mixture as tracer for the UDVP. In the case of turbidity currents the mixture was made by adding only sediments to clear water. Each experiment differs from the others in terms of the nature of the current, saline or turbidity, the value of the fractional excess density ($\Delta\rho/\rho$), the flow discharge at the inlet condition q_0, and bed roughness.

Every UDVP's probe employed in the experiments is able to acquire the instantaneous velocity profile along its axis in each section where is placed. Employing the DOP2000 in multiplexer mode, the system is not able to acquire velocity profiles from every probe simultaneously, but can only acquire in sequence from each probe. As

ESURFD
1, 817–853, 2013

a consequence the time between two consequent profiles at the same cross section is equal to the sum of the recording times of all the probes employed in the experiment.

In any cross section we employ the relations proposed by Ellison and Turner (1959) to evaluate the mean values of velocity U and height h of the current. They read:

$$Uh = \int_0^{z_\infty} u \mathrm{d}z \tag{1}$$

$$U^2 h = \int_0^{z_\infty} u^2 \mathrm{d}z \tag{2}$$

The upper limit of integration z_∞ is chosen as the height at which $u = 0.3U$. These flow properties were employed to scale the velocity profiles and also to evaluate the flow discharge per unit width q and the buoyancy flux per unit width B, defined as:

$$q = Uh \tag{3}$$

$$B = g'Uh \tag{4}$$

The experimental procedure is the same for all the experiments performed. In the two tanks (each characterized by a volume capacity of 2 m^3) the mixture was prepared adding to the fresh water the prescribed amount of salt and sediment, in order to obtain a fluid with the desired density. The fluid inside the tank was stirred by a mixer to avoid sediment deposition and density stratification inside the tank. Before starting the experiments, the flume was pre-filled with fresh water, and its density and temperature were measured such to determine the exact value of excess density between the mixture and the ambient fluid.

The flow discharge was adjusted before every experiment, using a recirculation conduit (Fig. 1) where a control valve was opened of an amount such to obtain the specified value of flow discharge. The experiment started when the valve of the flume conduit

ESURFD
1, 817–853, 2013

was opened such to feed the channel with the mixture. At the same time the bottom drain valve placed at the end of the flume was opened of an amount such to remove the same flow discharge from the system and to keep the free surface elevation constant in time during the experiment. Once the fluid mixture reaches the inlet chamber, that has a sluice gate at the bottom, the current starts flowing on the bed along the channel.

The head of the current starts moving downstream the flume through the first straight reach, proceeds along the bend and continues to the end of the channel. A few minutes after the head of the currents has passed, it is possible to observe that the current reaches a quasi-steady state. This is the time at which we start measurements of velocity profiles and we take fluid samples to determine the density distribution of the current. Depending on the value of flow discharge, each test had a different duration varying between about 10 and 30 min.

In Fig. 3 we report the temporal evolution of depth averaged velocity U and flow thickness h in cross section C5 where it is possible to notice the passage of the flow head, characterized by a rapid increase in flow thickness followed by a region where the flow is quasi-steady with minor temporal oscillations.

3 Observations on the structure of velocity and concentration profiles and global flow properties

3.1 Velocity profiles

Velocity profiles are obtained by performing averaging operations on the instantaneous profiles in a time interval of 10 s.

Figure 4 shows a typical example of the longitudinal velocity profile, once the time averaging operation has already been performed. The interface between the current and the clear water is located roughly 9 cm above the rigid bed. Moving up from the bottom we can notice that the velocity rapidly increases reaching the maximum located in the lower part of the current. Above the peak, the velocity invariably decreases approach-

ESURFD
1, 817–853, 2013

ing the current interface. Above the interface, there is still a small layer of ambient fluid which is dragged downstream by the underlying current, whereas above such fluid layer, a back flow is typically observed characterized by velocities much smaller than the underlying current.

The vertical structure of longitudinal velocity is not the same in the longitudinal direction. Starting from the inlet, where the shape of velocity profile is jet-like, the profiles attains a similar vertical distribution proceeding downstream where the flow is quasi-uniform. This is reported in Fig. 5 where we show a sequence of longitudinal velocity profiles evidencing the spatial development of the average velocity profiles in a typical saline current (experiment S4: $q_0 = 0.0034\,\mathrm{m^2\,s^{-1}}$, $\Delta\rho/\rho = 0.6\,\%$). Unfortunately the DOP was not able to measure the velocity profile in the region close to the sluice gate where the flow was supercritical. The cross section C1 closest to the inlet was already located in the region downstream from the hydraulic jump where the flow was already quasi-uniform. Every run has a similar behaviour, despite the flow thickness and velocity intensity change in different experiments.

The light blue line in Fig. 5 represents the interface between the current and the ambient fluid observed during the experiment. This was extracted by visually identifying the interface between the clear water and the turbid underflow. It is possible to observe that the interface is almost parallel to the bottom slope, thus suggesting that the current reaches a quasi-uniform condition quite close to the inlet. The blue dots are the values of the flow height h obtained by the averaged velocity profile, using the Eqs. (1) and (2); it is possible to notice the good correspondence between the elevation of flow interface computed from velocity profiles and that measured visually during the experiment. Not considering the profile close to the inlet and upstream from the hydraulic jump, in Fig. 6a the velocity profiles at different cross sections are compared. It is evident that the velocity changes only slightly proceeding downstream.

From the data acquired during each test it is possible to find out some average characteristics of the currents obtained some distance ahead from the flume inlet. Indeed, the flow is supercritical at the upstream cross section, but becomes quasi-

ESURFD
1, 817–853, 2013

uniform downstream the hydraulic jump forming a short distance from the flow entrance. In particular, from Table 1 it can be noticed that the densimetric Froude number $Fr_d = U/\sqrt{g'h}$, with $g' = g\Delta\rho/\rho$ representing the reduced gravity, remains supercritical in many cases, but is less than unity in some other cases.

Time averaged velocity profiles have been calculated in every measuring cross section. Both the longitudinal velocity and the vertical coordinate were then scaled employing the values of depth averaged velocity and flow thickness corresponding to Eqs. (1) and (2) in order to obtain dimensionless velocity profiles. It is evident from Fig. 6b that, neglecting the profile too close to the inflow condition, velocity profiles corresponding to the same experiment, once made dimensionless, tend to collapse on a narrow band. Far from the initial section where the flow structure is determined by inflow condition and by the presence of an hydraulic jump, the flow adjust to a quasi-uniform flow characterized by the existence of a self-similar velocity profile on the vertical. In the following we will consider the vertical profiles measured along the channel axis and corresponding to cross section C5 located 5.25 m far from the upstream inflow where the flow is fully developed and has attained a quasi-uniform configuration.

3.2 Flow discharge

From the calculation of the depth averaged velocity U and flow thickness h of the currents we calculated the flow discharge per unit width $q = Uh$ in every cross section velocity measurements were performed. It is possible to notice from Fig. 7 that, downstream from the hydraulic jump located close to the inlet, the current adjust its characteristics to a quasi-steady condition where flow discharge slightly increases downstream due to entrainment of clear water from above. Such increase in flow discharge is also reflected in a slight thickening of the current proceeding downstream, whereas flow velocity U tends to keep almost constant.

From the calculation of the flow discharge in the downstream direction it is possible to notice in Fig. 8 that all the experiments show a value of q greater then the inlet value. This is related to water entrainment from above, particularly intense in the first few me-

ESURFD
1, 817–853, 2013

ters after the supercritical inlet condition, where an hydraulic jump was present. Water entrainment from above was however different in the various experiments performed, highly dependent on the initial value q_0 imposed upstream. In particular series characterized by low values of q_0 maintain the flow discharge approximately constant along the flume, whereas the increase of flow discharge q proceeding downstream was more intense in those experiments with high values of q_0 at the inlet. This is related to the character of the current, more prone to entrain fresh water as the flow becomes more supercritical.

3.3 Head velocity

Once the experiment is started, the heavier fluid starts flowing under the ambient fluid. The front of the current is the place where the dense fluid coming from the body meet the still lighter fluid that fills the environment. This is a place of great turbulence, in which the most important phenomena of bed sediment erosion and mixing between the current and the ambient fluid take place (Allen, 1971; Middleton, 1993).

It is well know that the body of the current is faster than the head (Middleton, 1966a, b; Best et al., 2001). This is confirmed from our experiments as reported in Fig. 9, where we show that the average downstream body velocity is roughly 20 % greater than the head velocity.

Didden and Maxworthy (1982) proposed an empirical expression concerning the value of the head velocity U_f in constant flux gravity currents where the entrainment of ambient fluid is neglected. The authors related the head velocity with the volume flux per unit width q and the reduced gravity g' in the form:

$$U_f = C(g'q)^{1/3} \tag{5}$$

with C an order one constant. The value of the constant C was found by Özgökmen and Chassignet (2002) who performed a series of numerical experiments, with a two dimensional (x, z) non-hydrostatic model, providing a value $C = 1.05 \pm 0.1$. The relation

ESURFD
1, 817–853, 2013

proposed above is confirmed by our experimental results: in Fig. 10 the theoretical prediction (Eq. 5) is compared with the experimental velocity measured during our experiments. The theoretical prediction tends to slightly overestimate the experimental values of front velocity.

3.4 Density profiles

Density profiles are obtained from the measurements performed on the flow samples taken by the siphons. Each measure taken at different heights from the bottom provides the time averaged value of fluid density at that elevation: indeed every sample has a density value that is the mean temporal value on a time frame necessary to fill the sample (typically 10 min).

In Fig. 11a we show a comparison between the density profiles measured in the same cross section in 4 experiments of saline currents characterized by the same upstream discharge ($q_0 = 0.0026\,\mathrm{m^2\,s^{-1}}$) but different values of the excess density at the inlet. It can be immediately noticed that the maximum value of the excess density differs from the corresponding inlet condition. This is primarily due the strong mixing effect occurring close to the flow inlet in correspondence of the hydraulic jump and secondly to the water entrainment of ambient fluid downstream the hydraulic jump where the current has attained a quasi-uniform configuration. Though the entrainment has a secondary role compared with the mixing effects in the region close to the input section, it is responsible for current dilution in the downstream direction. The density distribution along the vertical, in all the experiments performed, has a similar structure: it is approximately constant in the dense current, and rapidly decreases in the region near the interface to reach the value equal to the ambient fluid further up along the vertical.

This if further demonstrated with Fig. 11b where the profiles of excess density are scaled with their depth averaged value and vertical distances are scaled with flow thickness. Changing the initial value of the density at the inlet section, profiles collapse on each other. Indeed, in the case of density currents density stratification on the vertical

ESURFD
1, 817–853, 2013

within the current is nearly absent. Conversely, if one observes Fig. 12, where it is represented a comparison between the profile of excess density of a saline current, and the corresponding profile of a turbidity current, we can see that the latter has a higher density in the lower part, while decreases gradually towards the interface. In the upper part of the profile in fact the saline flow has a higher density value. This fact is due to the presence of suspended sediments in side a turbidity currents, that tend to settle down and move the higher value of density profile towards the bottom. In the experiments performed the sediments were very fine (d_s = 50 µm), this could be the reason why this tendency is not very clear. Also, it is worth pointing out that the samples taken with the syphons are affected by a measuring error larger than the differences in excess density that we would like to detect with the present comparison.

4 Velocity profiles under quasi-uniform conditions

Our attention is here focused on the quasi-steady conditions attained by the current some time after the passage of the current head. As already pointed out the body of the current is characterized by a quasi-uniform flow condition. Velocity measurements are recorded during the whole duration of each experiment, including the head. However, here we just consider velocity measurements corresponding to the body of the current. Similarly, density measurements are sampled in the body of the current.

4.1 Effect of the Reynolds number

One of the crucial parameters affecting the structure of the current is the Reynolds number of the current. To quantify its effects on the velocity profile we varied flow discharge at the inlet. Indeed the Reynolds number *Re* is proportional to the specific flow rate q in the form:

$$Re = \frac{Uh}{\nu} = \frac{q}{\nu} \tag{6}$$

ESURFD
1, 817–853, 2013

where v is the kinematic viscosity of the fluid and U and h are respectively the average velocity and height of the currents, calculated in the cross section from the longitudinal velocity profile.

We show in Fig. 13a the vertical profiles of different saline experiments performed by keeping the value of the excess density at the inlet constant and equal to 0.3 %. It is evident that increasing the flow rate the velocity intensity increases and simultaneously the current becomes thicker. However from this graph is not possible to find out some common characteristics, differences and analogies are more clearly evidenced if we scale all velocity profiles measured in the fully developed region with their characteristic values of velocity U and flow thickness h. They are reported in Fig. 13b, with colors corresponding to different experiments; furthermore the series have been indicated according to the Reynolds number of the current.

In Fig. 13b is possible to distinguish two different shapes of the velocity profiles. In particular currents characterized by a low value of the Reynolds number (red and green lines) exhibit a velocity maximum related to their averaged value higher than the series with higher value of Re. As a direct consequence the former shape results to be sharper then the further.

It is also possible to observe that there is a difference in the part of the velocity profiles up to the peak; in particular the concavity is upwards for low Re and opposite in the other case. Moreover, the part of the external ambient fluid that follows the flow in the downstream direction, compared to the thickness of the currents itself, increases with decreasing value of the Reynolds number of the flow.

4.2 Effect of the presence of suspended sediments

Although the fuel that induces and sustains these kind of phenomena is the difference in density between the flow and the ambient fluid, density currents show a different behavior whether they are induced by the presence of dissolved salt or suspended sediment. The reason for this difference is related two aspects. The first is due to the well known effect of suspended sediments on turbulence dumping. Indeed, in a clas-

ESURFD
1, 817–853, 2013

sical paper of open channel flows, Vanoni (1946) documented experimentally that an increase in the mean concentration of suspended sediment was associated with an increasing velocity gradient at the wall. It was first hypothesized and then confirmed by both theoretical investigations (Villaret and Trowbridge, 1991; Herrmann and Madsen, 2007; Bolla Pittaluga, 2011) and experimental observations (Muste et al., 2009) that the latter effect might originate from suspended sediments damping turbulence and decreasing turbulent mixing. The second reason is related to sediment entrainment from the bed. Both saline and turbidity currents, indeed, can modify their density entraining ambient fluid that dilutes them from above. In the case of sediment laden currents, however, the flow can also exchange sediments with the erodible bed either decreasing bulk density through sediments deposition or, vice versa, increasing bulk density through erosion from the bed of the submarine canyon.

Figure 14 shows the difference in the velocity profile between a saline (S14 red line) and a turbidity (S25 green-line) current in two experiments performed under the same conditions with the exception of the way the same value of excess density was generated (salt or sediments). It can be immediately noticed that the shape of the two dimensionless profiles shows some significant differences. Sediment laden flows have an higher value of velocity, compared with the averaged one, that is located closer to the bed; as a consequence the velocity profile appears quite sharp at the velocity peak. On the contrary the flow speed of the saline current is more spread on the vertical, resulting in a flatter velocity distribution characterized by a lower value of peak velocity compared to the previous case. Finally in the turbidity current case, velocity gradually decreases with distance from the interface whereas the velocity gradient is much more abrupt in the case of the saline current.

4.3 Effect of bed roughness

We also investigated the effects of the presence of a rough bed on the velocity distribution. Most of the experiments performed were carried out on a smooth plane bed. We then performed a new set of experiments placing a uniform layer of fine gravel, char-

ESURFD
1, 817–853, 2013

acterized by a $d_{50} = 3\,\text{mm}$, on the smooth fixed bed. The sediment size was chosen sufficiently rough such that particles remained fixed during the flow event.

Results are shown in Fig. 15 where we compare two classes of density currents performed under the same excess density at the inlet ($\Delta\rho/\rho_0 = 0.6\,\%$), similar values of flow discharge at the inlet ($q_0 = 0.0034-0.0069\,\text{m}^2\,\text{s}^{-1}$) but over a smooth (experiments S4, S23, S25) and a rough bed (experiments S26, S27, S28), respectively.

We first noticed that differences in velocity profiles between the two cases were evident. Primarily the maximum speed of the current was grater and located closer to the bed in the smooth configuration respect to the rough case. The velocity intensity at the bottom was reduced as a results of increased bed friction; in addition the velocity profile increased its thickness.

Observing Fig. 15 it is interesting to note that the dimensionless longitudinal velocity is characterized by a velocity peak that is higher in the rough bed experiment respect to the smooth one. Indeed, the height of the velocity peak moves from roughly $0.25h$ in the smooth case to roughly $0.4h$ in the rough case. Also, the dimensionless flow velocity is slightly reduced in the lower part close to the bed, as a consequence of the increase in bed resistance, and is slightly faster above the velocity peak. It is also worth noting that the two profiles show the same value of the maximum dimensionless velocity (u_{max}/U) and that the elevation of the interface is not affected significantly by the change in bed roughness.

4.4 Effect of excess density

Another aspect that we wanted to investigate is the effect of the value of the excess density on the velocity profile. We then performed three saline experiments generating currents characterized by different values of excess density and keeping all the other input values constant. Figure 16a shows that, increasing the value of excess density, the flow increases the peak velocity, and also the depth averaged velocity, and at the same time becomes thinner with a velocity peak closer to the bottom. Although it is evident the effect that an increase in density has on the current (Fig. 16a), observing

ESURFD
1, 817–853, 2013

the dimensionless profiles in Fig. 16b the shape of the velocity profiles do not seem to be affected by this change. It should be noted however that the variations of excess density are small, as they are limited to a few percent. They are then sufficient to influence the overall flow dynamics of the current but the values of excess density are not large enough to produce significant changes on the dimensionless shape of longitudinal velocity. This suggests that the excess density is, among the parameters here considered and in the range of variation here employed, the one that has a smaller influence on the shape of the longitudinal velocity profiles.

4.5 Effect of the densimetric Froude number

Finally we investigate the influence of the densimetric Froude number Fr_d on the velocity profile. We selected the experiments characterized by different values of Fr_d but similar characteristic of the other parameters examined before. In particular they have a value of Re larger than 4.8×10^3 up to a maximum of 15×10^3, they are all saline currents flowing on a smooth bed. The experiments considered here have a value of Fr_d falling in the range 0.65–0.88 for the subcritical flows, and in the range 1.07–1.18 for the supercritical cases. As it can be seen from the Fig. 17 the dimensionless profiles of velocity do not show an evident difference related to the character of the current (subcritical or supercritical). According to the present experimental observations, the densimetric Froude number does not affects significantly the dimensionless shape of the velocity profile.

5 Conclusions

In this work we reported the results of 27 experiments on turbidity and saline density currents. Every experiments was performed by changing either the value of flow discharge at (q_0) at the inlet, or the fractional excess density ($\Delta\rho/\rho$) at the inlet, or the way in which the excess density was generated (with salt or sediments) or, finally,

ESURFD
1, 817–853, 2013

the roughness of the bed. We were interested in quantifying how these parameters affect the dynamics of the current flowing in a straight channel, and if it was possible to identify some dimensionless parameter responsible for the vertical shape of the dimensionless longitudinal velocity. Indeed we focused our attention on the development of the currents in the first straight reach of our flume, where we observed the achievement of a quasi-uniform state of the current characterized by self-similar dimensionless velocity profiles. Their turned out to be affected by the Reynolds number of the flow, by the relative bed roughness and by the presence of sediment in suspension. The densimetric Froude number, apparently, turned out to have a negligible effect on the vertical structure of the dimensionless velocity profile. More specifically, currents with low values of the Reynolds number were characterized by sharper profiles close to the peak velocity with respect to those corresponding to large values of the Reynolds number. The presence of suspended sediment in the currents, which distinguish turbidity from saline currents, was responsible for the downward movement of the peak velocity; this was due to the natural property of the sediments to settle down. On the contrary, increasing the bed roughness we observed that the peak velocity was higher with respect case of smooth bed.

We are presently extending the measurements to the curved bend, located downstream from the first straight reach in order to investigate the vertical structure of secondary flow in currents flowing in a constant curvature bend, and their possible influence on the structure of longitudinal velocity as well as on the overall dynamics of the current.

Acknowledgements. Partial funding provided by the University of Genova within the project "Morphodynamics of turbidity currents flowing in submarine meandering channels" (Progetto di Ateneo, 2011) and by Shell International Exploration and Production is gratefully acknowledged. This work is also part of the Ph.D. thesis of M. Stagnaro to be submitted to the University of Genova in partial fulfillment of his degree.

ESURFD
1, 817–853, 2013

References

Allen, J. R. L.: Mixing at turbidity current heads, and its geological implications, J. Sediment. Res., 41, 97–113, 1971. 826

Altinakar, M., Graf, W., and Hopfinger, E.: Weakly depositing turbidity current on a small slope, J. Hydraul. Res., 28, 55–80, 1996a. 819

Altinakar, M., Graf, W., and Hopfinger, E.: Flow structure in turbidity currents, J. Hydraul. Res., 34, 713–718, 1996b. 819

Best, J. L., Kirkbride, A. D., and Peakall, J.: Mean Flow and Turbulence Structure of Sediment-Laden Gravity Currents: New Insights Using Ultrasonic Doppler Velocity Profiling, Blackwell Publishing Ltd., 157–172, 2001. 826

Bolla Pittaluga, M.: Stratification effects on flow and bed topography in straight and curved erodible streams, J. Geophys. Res., 116, F03026, doi:10.1029/2011JF001979, 2011. 830

Didden, N. and Maxworthy, T.: The viscous spreading of plane and axisymmetric gravity currents, J. Fluid Mech., 121, 27–42, 1982. 826, 846

Ellison, T. H. and Turner, J. S.: Turbulent entrainment in stratified flows, J. Fluid Mech., 6, 423–448, doi:10.1017/S0022112059000738, 1959. 822

Herrmann, M. J. and Madsen, O.: Effect of stratification due to suspended sand on velocity and concentration distribution in unidirectional flows, J. Geophys. Res., 112, C02006, doi:10.1029/2006JC003569, 2007. 830

Middleton, G. V.: Experiments on density and turbidity currents: I. Motion of the head, Can. J. Earth Sci., 3, 523–546, 1966a. 826

Middleton, G. V.: Experiments on density and turbidity currents: II. Uniform flow of density currents, Can. J. Earth Sci., 3, 627–637, 1966b. 826

Middleton, G. V.: Sediment deposition from turbidity currents, Annu. Rev. Earth Pl. Sc., 21, 89–114, 1993. 826

Muste, M., Yu, K., Fujita, I., and Ettema, R.: Two-phase flow insights into open-channel flows with suspended particles of different densities, Environ. Fluid. Mech., 9, 161–186, 2009. 830

Özgökmen, T. M. and Chassignet, E. P.: Dynamics of two-dimensional turbulent bottom gravity currents, J. Phys. Oceanogr., 32, 1460–1478, 2002. 826

Sequeiros, O., Spinewine, B., Beaubouef, R., Sun, T., García, M., and Parker, G.: Characteristics of velocity and excess density profiles of saline underflows and turbidity currents flowing over a mobile bed, J. Hydraul. Eng., 136, 412–433, 2010. 819

ESURFD
1, 817–853, 2013

Vanoni, V. A.: Transportation of suspended sediment in water, Trans. Am. Soc. Civ. Eng., 111, 67–133, 1946. 830

Villaret, C. and Trowbridge, J. H.: Effect of stratification by suspended sediments on turbulent shear flows, J. Geophys. Res., 96, 10659–10680, 1991. 830

Xu, J. P., Noble, M. A., and Rosenfeld, L. K.: In-situ measurements of velocity structure within turbidity currents, Geophys. Res. Lett., 31, L09311, doi:10.1029/2004GL019718, 2004. 819

ESURFD

1, 817–853, 2013

Table 1. Summary of the principal characteristics of the 27 experiments performed.

Exp. no.	Excess density $\Delta\rho/\rho$	Flow discharge q_0 ($m^2 s^{-1}$)	Mixture salt–sand (%)	Average velocity U ($m s^{-1}$)	Average flow depth h (m)	Densimetric Froude n. Fr_d	Reynolds number $Re \times 10^3$	Bed roughness (–)
S1	0.023	0.0034	90–10 %	0.086	0.069	0.88	5.6	smooth
S2	0.012	0.0034	90–10 %	0.063	0.081	0.65	4.8	smooth
S3	0.012	0.0034	0–100 %	0.074	0.069	0.82	4.8	smooth
S4	0.006	0.0034	90–10 %	0.072	0.087	1.10	5.9	smooth
S5	0.003	0.0009	90–10 %	0.022	0.047	0.59	0.98	smooth
S6	0.003	0.0017	90–10 %	0.043	0.061	1.01	2.5	smooth
S7	0.003	0.0026	90–10 %	0.060	0.085	1.47	4.8	smooth
S8	0.004	0.0121	90–10 %	0.084	0.185	0.99	15.0	smooth
S9	0.004	0.0069	90–10 %	0.074	0.160	1.08	11.0	smooth
S10	0.023	0.0069	90–10 %	0.106	0.093	0.91	9.3	smooth
S11	0.013	0.0069	90–10 %	0.106	0.091	1.07	9.1	smooth
S12	0.013	0.0009	90–10 %	0.043	0.036	0.69	1.5	smooth
S13	0.013	0.0017	90–10 %	0.061	0.047	1.00	2.7	smooth
S14	0.006	0.0069	90–10 %	0.075	0.168	1.07	12.0	smooth
S15	0.006	0.0009	90–10 %	0.034	0.036	0.81	1.2	smooth
S16	0.006	0.0017	90–10 %	0.054	0.044	1.16	2.2	smooth
S17	0.004	0.0034	90–10 %	0.056	0.115	1.18	6.1	smooth
S18	0.006	0.0026	90–10 %	0.054	0.079	0.97	4.0	smooth
S19	0.012	0.0026	90–10 %	0.071	0.056	1.01	3.8	smooth
S20	0.023	0.0026	90–10 %	0.087	0.043	1.06	3.5	smooth
S21	0.023	0.0009	90–10 %	0.044	0.026	0.80	1.1	smooth
S22	0.023	0.0017	90–10 %	0.059	0.042	0.75	2.3	smooth
S23	0.006	0.0034	0–100 %	0.056	0.114	0.97	6.0	smooth
S25	0.006	0.0069	0–100 %	0.073	0.153	1.09	11.0	rough
S26	0.006	0.0034	0–100 %	0.049	0.122	1.42	5.6	rough
S27	0.006	0.0069	0–100 %	0.061	0.167	0.87	9.6	rough
S28	0.006	0.0034	90–10 %	0.063	0.091	1.05	5.4	rough

ESURFD
1, 817–853, 2013

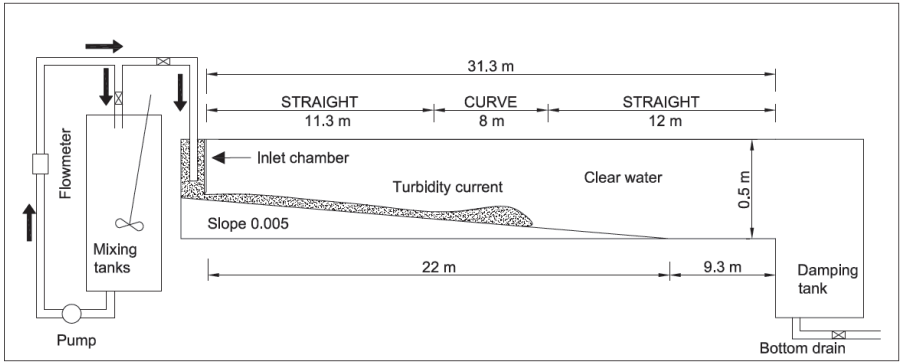

(a)

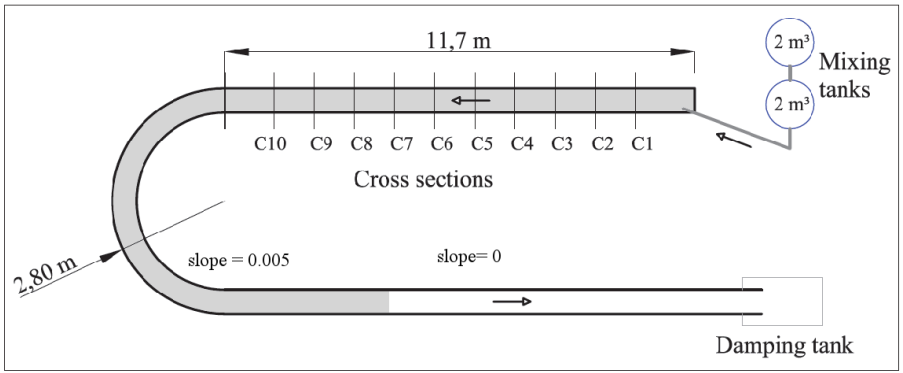

(b)

Fig. 1. (a) Sketch and **(b)** plan view of the turbidity current flume.

ESURFD
1, 817–853, 2013

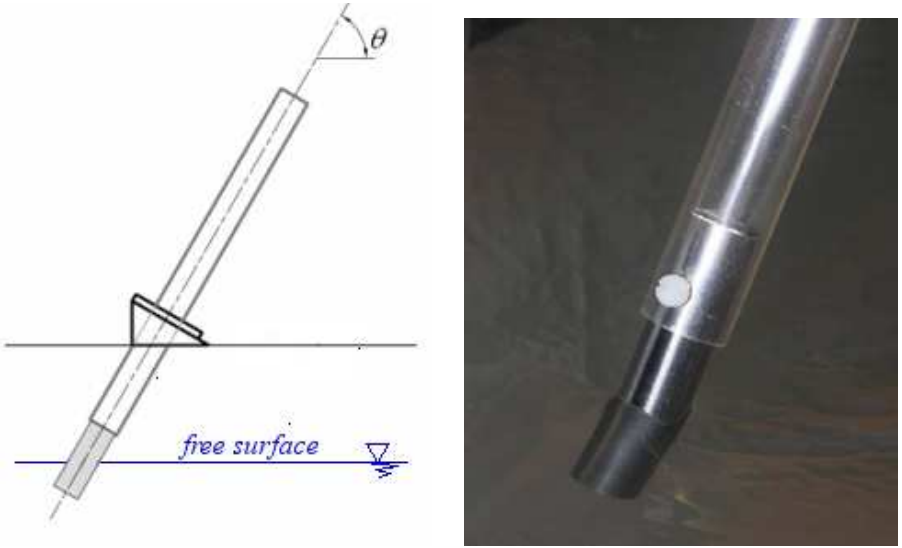

Fig. 2. DOP2000 probe: **(a)** scheme of the probe installation, and **(b)** the probe in operation during one experiment.

ESURFD
1, 817–853, 2013

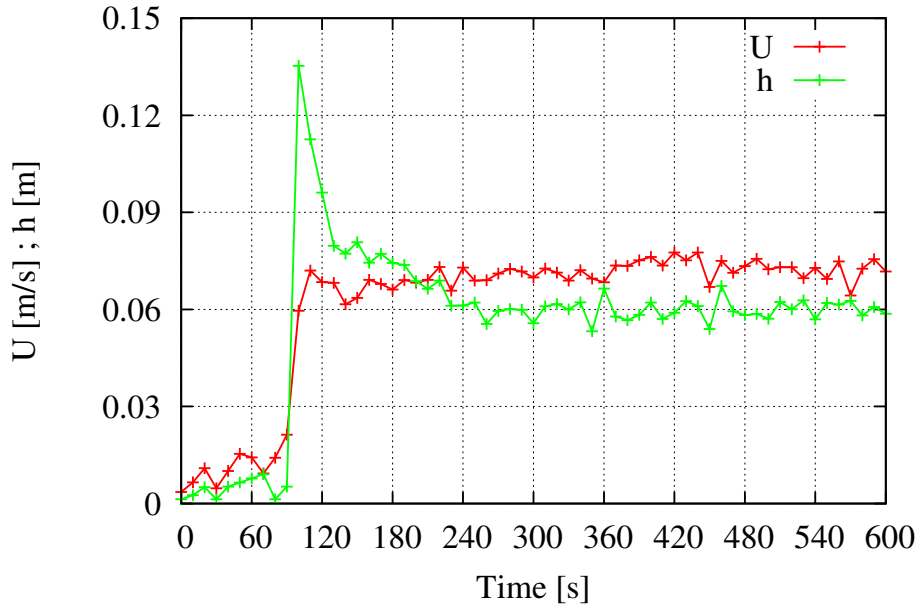

Fig. 3. Experiment S4: time evolution of the mean velocity and the mean height of the current in cross section C5.

ESURFD
1, 817–853, 2013

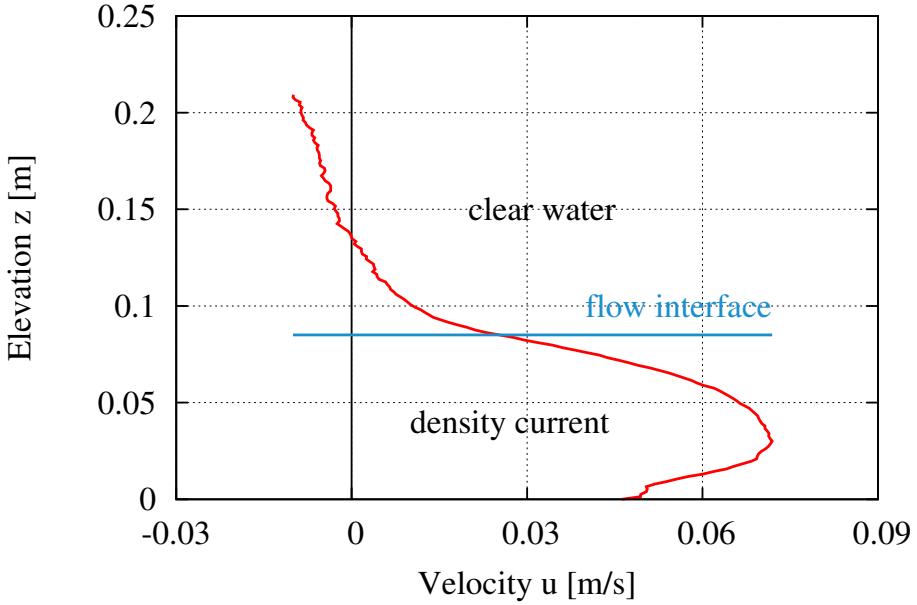

Fig. 4. Example of a longitudinal velocity profile once the time averaging operation has been performed. Experiment S7 ($q_0 = 0.0026\,m^2\,s^{-1}$ and $\Delta\rho/\rho = 0.3\,\%$) at cross section C5.

ESURFD
1, 817–853, 2013

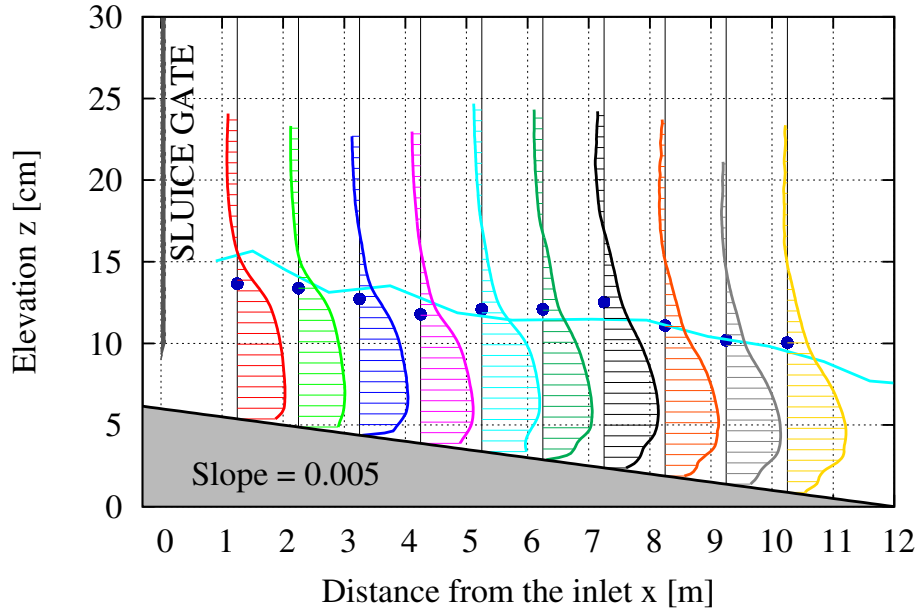

Fig. 5. Spatial distribution of velocity profiles measured in experiment S4 (Saline flow, q_0 = 0.0034 $m^2 s^{-1}$, $\Delta\rho/\rho$ = 0.6 %). The flow interface (blue line) measured during the experiment is also represented as well as the interface height obtained from the corresponding velocity profile (blue dots) employing Eqs. (1) and (2).

ESURFD
1, 817–853, 2013

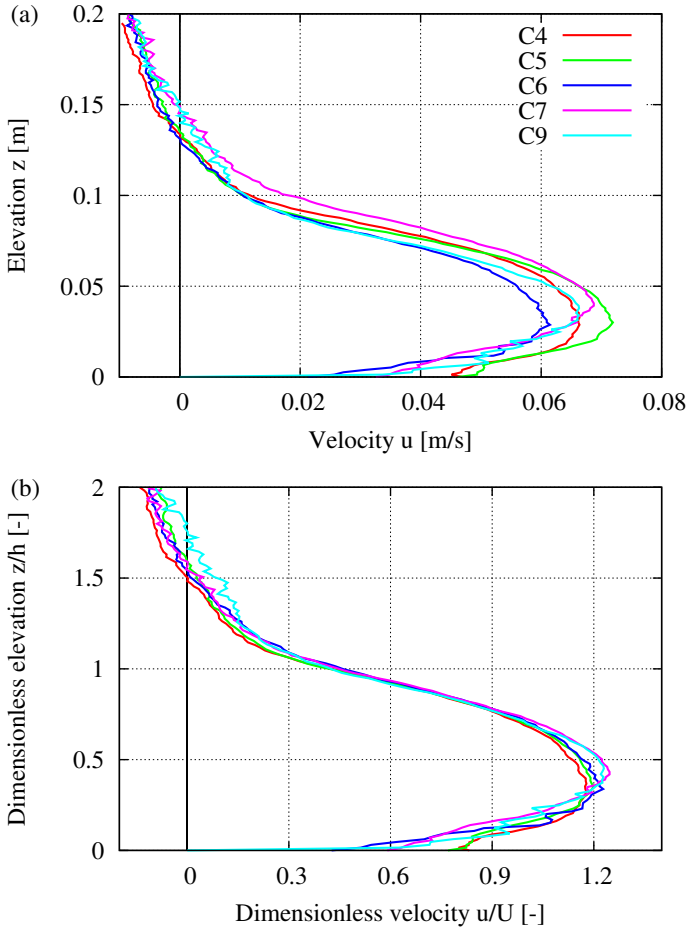

Fig. 6. Example of velocity profiles: **(a)** dimensional velocity profiles and **(b)** dimensionless velocity profiles in different cross section from experiment S7 ($q_0 = 0.0025\,\mathrm{m^2\,s^{-1}}$; $\Delta\rho/\rho = 0.3\,\%$).

ESURFD
1, 817–853, 2013

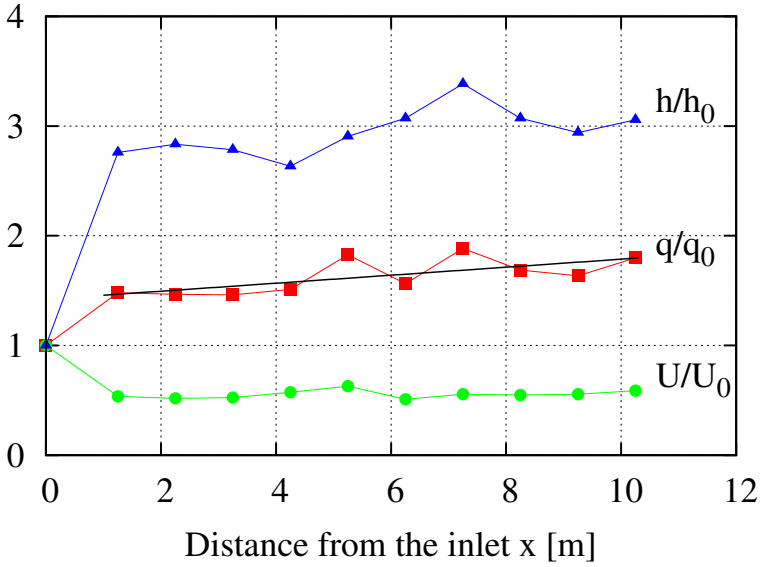

Fig. 7. Experiment S4: spatial development of the mean velocity, mean height and flow discharge of the current, compared with their initial value.

ESURFD
1, 817–853, 2013

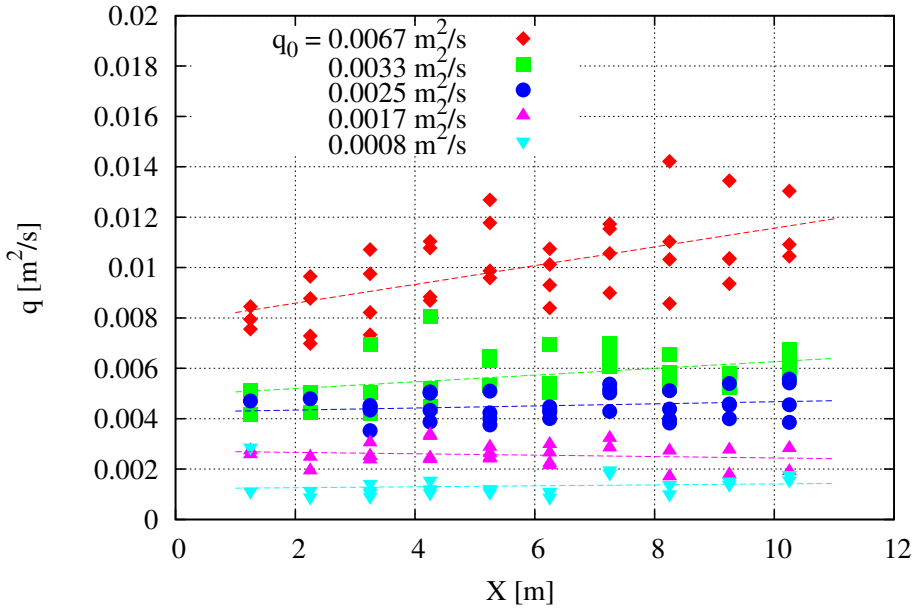

Fig. 8. Flow discharge: spatial distribution of flow discharge per unit with $q(x)$ along the flume and corresponding linear regression.

ESURFD
1, 817–853, 2013

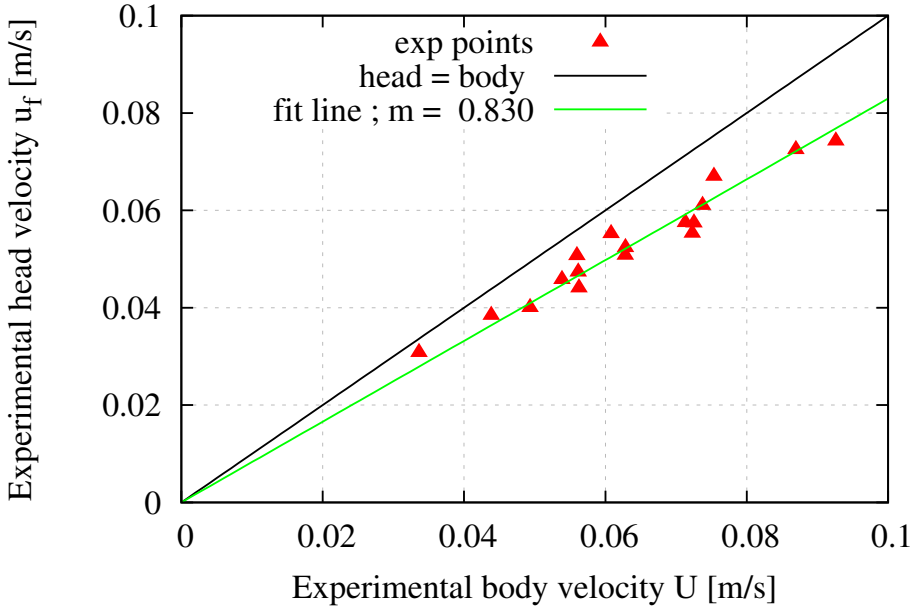

Fig. 9. Comparison between the value of the experimental head velocity and the value of the velocity of the body averaged in time.

ESURFD
1, 817–853, 2013

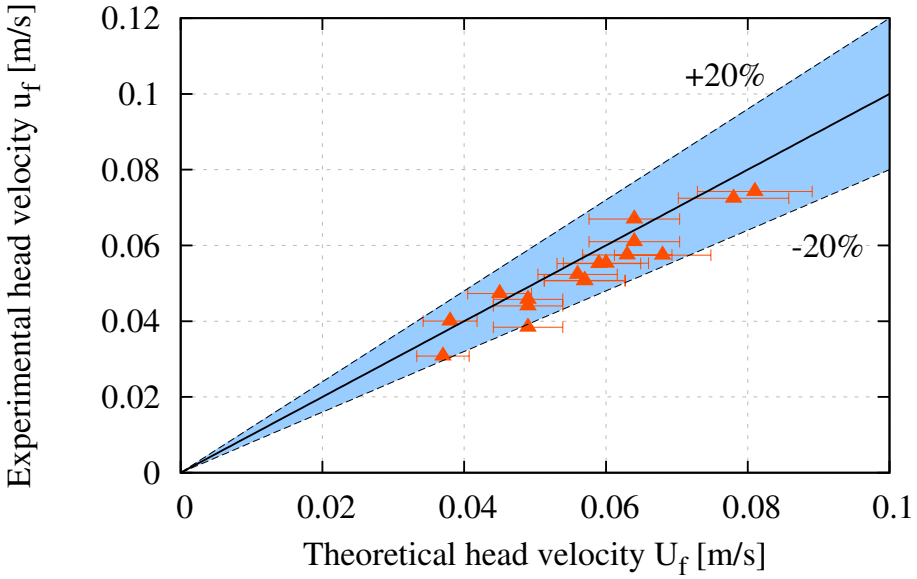

Fig. 10. Comparison between the experimental values and the theoretical predictions obtained by the empirical expression proposed by Didden and Maxworthy (1982) with C = 1.05.

ESURFD
1, 817–853, 2013

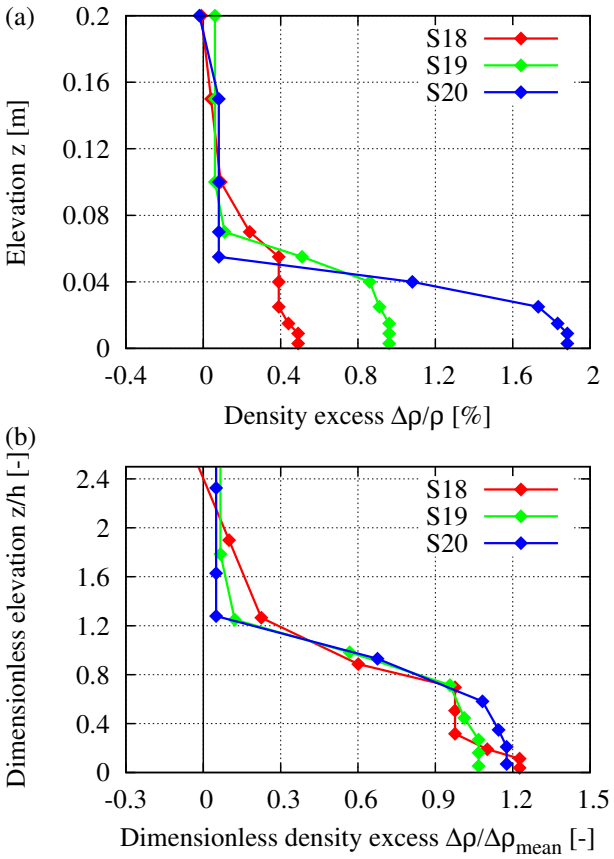

Fig. 11. Dimensional **(a)** and dimensionless **(b)** density profiles: comparison between series with different inlet condition of density excess, and same value of flow discharge q_0 = 0.0017 $m^2 s^{-1}$, measured in C5 cross section.

ESURFD
1, 817–853, 2013

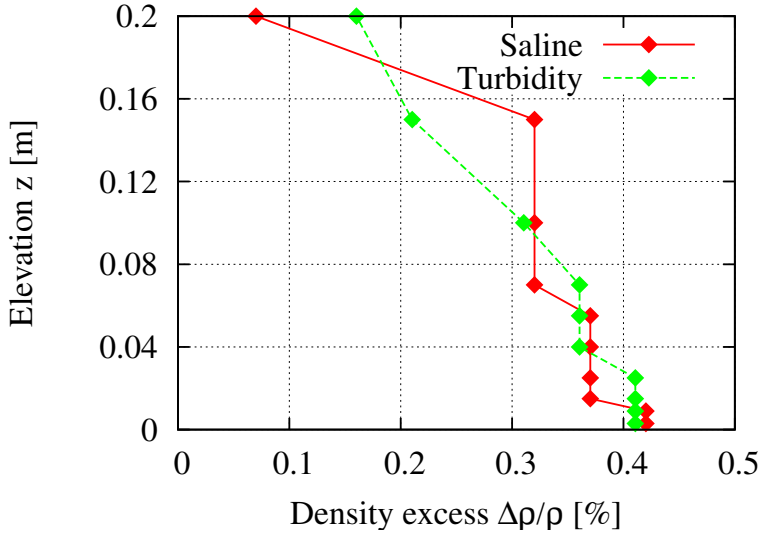

Fig. 12. Density profiles: comparison between a saline current (experiment S14) and a turbidity current (experiment S25), measured in cross section C5.

ESURFD
1, 817–853, 2013

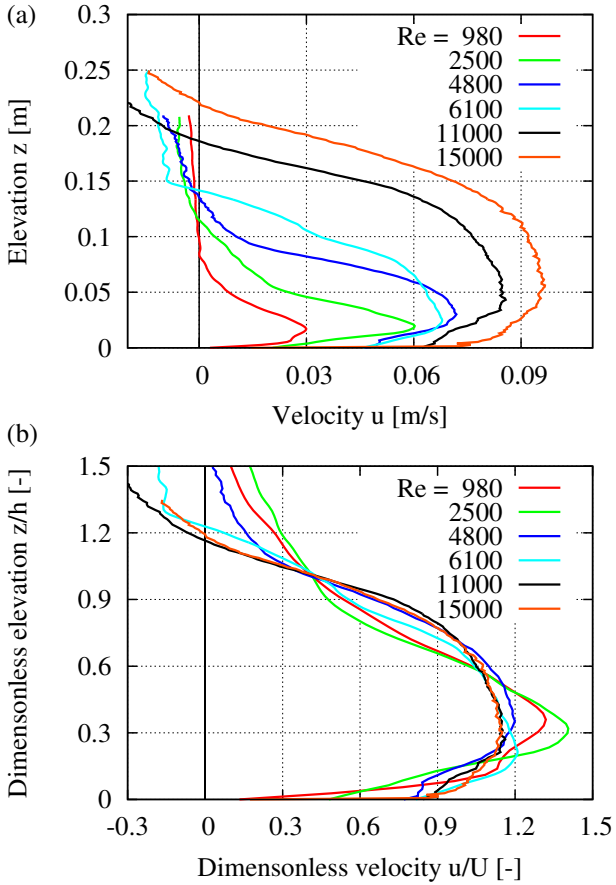

Fig. 13. Dimensional **(a)** and dimensionless **(b)** averaged velocity profiles: effects of the variation of the flow rate q; saline currents with $\Delta\rho/\rho = 0.3\%$ measured in cross section C5 (experiments S5, S6, S7, S17, S9 and S8).

ESURFD
1, 817–853, 2013

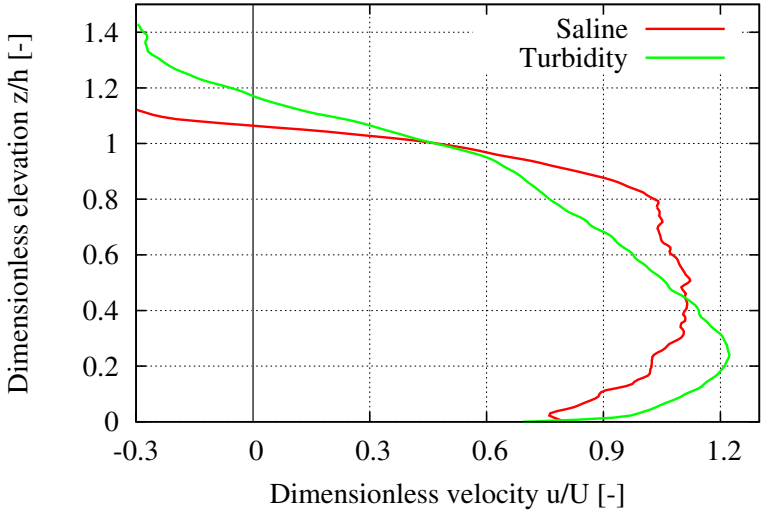

Fig. 14. Comparison between a saline density current (experiment S14) and a turbidity current (experiment S25) with suspended sediment performed under the same conditions (q_0 = 0.0069 $m^2 s^{-1}$ and $\Delta\rho/\rho_0$ = 0.6 %), measured in cross section C5.

ESURFD
1, 817–853, 2013

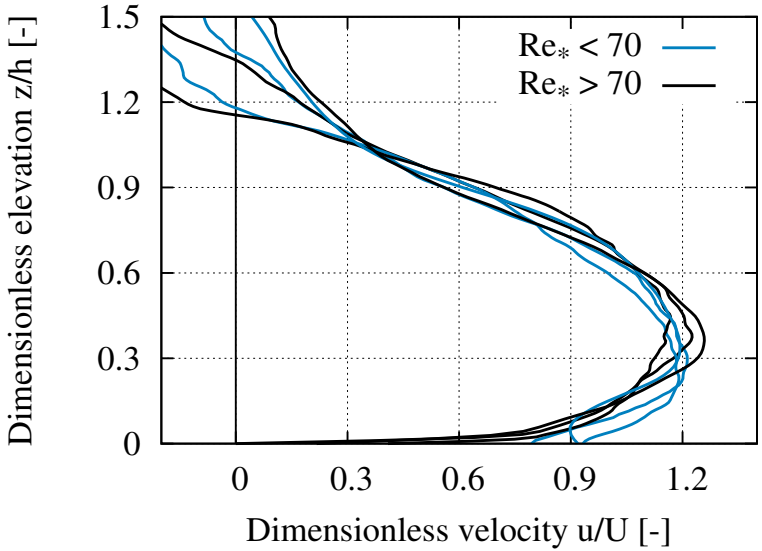

Fig. 15. Comparison between density currents flowing over a smooth (experiments S4, S23, S25) and rough (experiments S26, S27, S28) bed.

ESURFD
1, 817–853, 2013

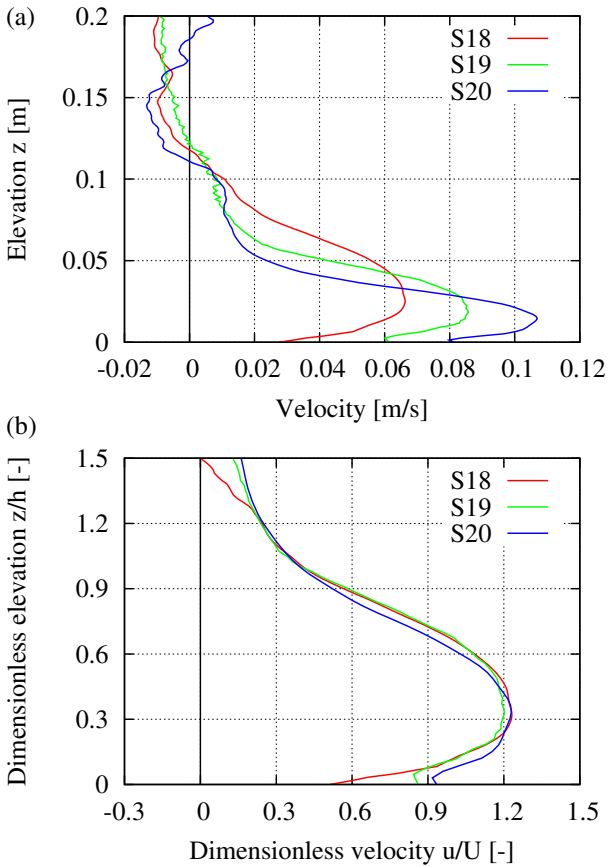

Fig. 16. Dimensional **(a)** and dimensionless **(b)** comparison between density current velocity profiles with different density excess ($\Delta\rho/\rho$) and same flow discharge ($q_0 = 0.0026\,m^2\,s^{-1}$) at the inlet (experiments S18, S19 and S20).

ESURFD
1, 817–853, 2013

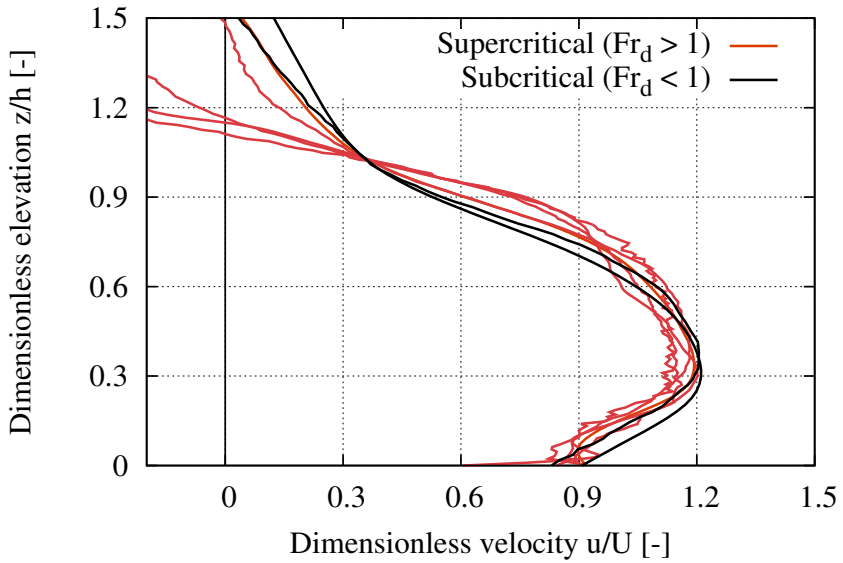

Fig. 17. Comparison between subcritical ($Fr_d < 1$) and supercritical ($Fr_d > 1$) experiments.

ESURFD
1, 817–853, 2013